Parallel and perpendicular multilayer relaxation of Fe{310}

J. Sokolov* and F. Jona

Department of Materials Science and Engineering, State University of New York, Stony Brook, New York 11794

P. M. Marcus

IBM Research Center, P.O. Box 218, Yorktown Heights, New York 10598

(Received 29 November 1983)

We report the results of a low-energy electron-diffraction analysis of the atomic structure of the {310} surface of body-centered-cubic iron. Damped relaxations from bulklike structure are found in the directions both parallel and perpendicular to the surface and extending four layers deep into the lattice. The surface structure is as follows: first interlayer spacing $d_{12}=0.76\pm0.03$ Å (bulk value is 0.906 Å), second interlayer spacing $d_{23}=1.02\pm0.03$ Å, third interlayer spacing $d_{34}=0.87\pm0.04$ Å, change of first-to-second layer registry shift $\Delta a_{12}=0.13\pm0.05$ Å, and change of second-to-third layer registry shift $\Delta a_{23}=0.03\pm0.05$ Å. Both changes of registry shifts are in the same direction, along a $\langle 310\rangle$ axis, and cause a decrease in the difference between nearest- and next-nearest-neighbor distances between atoms in adjacent layers.

I. INTRODUCTION

Renewed interest in surface structure of metals has developed in the last few years as advances in both surface theory and experimental techniques have revealed considerable complexity in the relaxation of the outermost atomic layers. Calculations have predicted,[1,2] and a number of experiments have shown,[3-10] deviations from bulklike structure extending several layers deep. Structures for low-index faces exhibit a characteristic damped oscillatory relaxation of interlayer spacings (i.e., changing sign from layer to layer). Recently, with the case of Fe{211},[10] we have demonstrated that on surfaces less symmetrical than the commonly studied {001}, {110}, and {111} surfaces, multilayer relaxations involving motion of atoms parallel to the surface occur and, for the {211} surface at least, these relaxations are also oscillatory. However, the pattern of relaxations on surfaces of lower symmetry, i.e., the *signs* of the interlayer relaxations and the registry shifts, appear to vary from surface to surface for the three cases which have now been studied: Fe{211}, Fe{210},[11] and Fe{310}. It is this complexity, which is a function of both electronic and atomic structure near the surface and which provides a test for theories of metal surfaces, that makes these cases very interesting. By essentially doubling the amount of experimental information—the relaxation of each atomic layer now has two components, one parallel and one perpendicular to the surface—the test of theories of surface structure by comparison of observed and predicted structures is made more stringent. Fe{310} was chosen for study because it is a quite open, or rough, surface (packing fraction[12] 0.3725) with low symmetry (only one mirror plane); these properties make it a favorable candidate for multilayer relaxation. Section II describes the experimental methods, Sec. III briefly outlines the calculations, and Sec. IV presents the structure analysis of the low-energy electron-diffraction (LEED) intensity data by means of experiment-theory comparison, using the reliability factor (r factor) of Zanazzi and Jona.[13]

II. EXPERIMENTAL SETUP

The Fe{310} sample was spark-cut from a single-crystal specimen grown by strain-annealing of ultrapure source material provided by the American Iron and Steel Institute (for details see Ref. 14). Laue photographs were used to orient the sample to within $\pm0.5°$ of the {310} plane. The crystal was then ground and mechanically polished with water-based alumina slurries (smallest bead size 0.3 μm).

The following steps were required to obtain a clean surface in ultrahigh vacuum (base pressure about 7×10^{-11} Torr): (i) room-temperature Ar$^+$ bombardment (2–4 μA at 400 eV) for 2 h, (ii) Ar$^+$ bombardment with sample temperature raised to 850 °C for 2 h, followed by a 1-h anneal at the same temperature, and (iii) a series of Ar$^+$ bombardments for 2–3 h each with sample temperature at 400–500 °C followed by 1-h anneal at 600–650 °C (total time of argon treatments approximately 25 h). Auger spectroscopy was used to monitor surface cleanness; sulfur, oxygen, and carbon were the main impurities before cleaning. After cleaning, surface cleanness was comparable to our previous iron work.[15]

Thirty-three low-energy electron-diffraction (LEED) spectra (intensity-versus-energy curves, 21 nondegenerate) were collected by means of a spot-photometer, the sample being held at room temperature for all measurements: fourteen spectra at normal incidence (10, 0$\bar{1}$, $\bar{1}$0, 01, 1$\bar{1}$, $\bar{1}$1, 2$\bar{1}$, 1$\bar{2}$, 2$\bar{2}$, $\bar{2}$2, $\bar{3}$2, $\bar{2}$3, 3$\bar{2}$, and 2$\bar{3}$), ten spectra at $\theta=7°$, $\phi=-107.5°$ (00, 10, 0$\bar{1}$, $\bar{1}$0, 01, $\bar{1}$1, $\bar{1}$2, $\bar{2}$1, 2$\bar{3}$, and 3$\bar{2}$), and nine spectra at $\theta=14°$, $\phi=-107.5°$ (00, 10, 0$\bar{1}$, $\bar{1}$0, 01, $\bar{1}$1, 2$\bar{1}$, 1$\bar{2}$, and 2$\bar{3}$). Angles and beam indices follow the convention of Zanazzi *et al.*[16] Figure 1 shows a schematic representation of the LEED pattern.

The method used to determine the condition of normal incidence of the incoming electron beam on the sample was the following: (i) orient the crystal so that the incoming beam is in the {100} mirror plane normal to the surface by adjusting the sample position until the beams with indices xy and $\bar{y}\bar{x}$ in Fig. 1 (with x,y equal to 0,1,2,3,...)
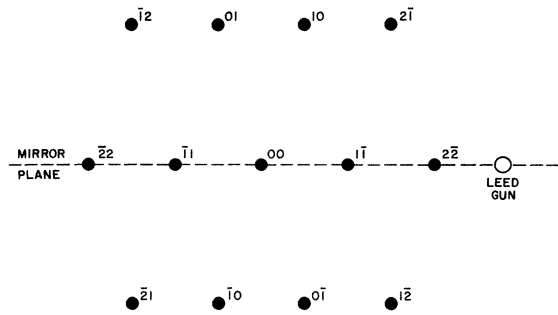
FIG. 1. Schematic LEED pattern from Fe{310} for $\theta \neq 0°$ and $\phi = -107.5°$.

give, as nearly as possible, identical $I\text{-}V$ spectra, and (ii) keeping the incoming beam in the {100} mirror plane, rotate the sample by various angles θ such that the 00 scattered beam appears on the fluorescent screen on both sides of the electron gun (located at the center of the screen) and record the corresponding I-V spectra of the 00 beam at each angle; by symmetry, for equal θ on opposite sides of the LEED gun the 00 spectra will be identical and can thus be used to determine the condition $\theta = 0°$.

III. CALCULATIONS

Dynamical LEED intensity calculations were done with the computer program CHANGE (described in Refs. 17 and 18). The Fe potential was the same as used successfully for studies of other iron surfaces (for example, Legg et al.[19]). The inner potential was taken as energy independent; the imaginary part β of the potential was set equal to 4 eV and the real part V_0 was to be determined from the intensity analysis; the initial value was fixed at -11.5 eV. The mean atomic vibrational amplitude was taken as $(\langle u^2 \rangle)^{1/2} = 0.115$ Å and eight phase shifts were

used to represent the ion core scattering. Occasionally, some troublesome numerical instabilities were encountered (blowups, i.e., very large intensity values, and unphysical kinks in the calculated curves), presumably due to the small interlayer spacings of Fe{310} ($d_{\text{bulk}} = 0.906$ Å). The main remedy was to bunch together layers into slabs three or four layers thick, with scattering within the slabs done in the angular momentum basis (which has no limitations in handling closely spaced layers) and scattering between slabs done in the plane-wave basis. Up to 65 plane waves, or beams, were used in the calculations. At 245 eV, 65 beams are propagating.

IV. STRUCTURE ANALYSIS

Top and side views of the outer atomic layers of a bulk-like Fe{310} surface are shown in Fig. 2, and various surface parameters are defined in Table I. The surface is quite open, with a packing fraction[12] of 0.3725 (the close-packed bcc {110} face has a packing fraction of 0.8330). The surface unit mesh is a parallelogram formed by mesh vectors $\vec{a}_2$, directed along a $\langle 100 \rangle$ axis and of length 2.87 Å, and $\vec{a}_1$, directed along a $\langle 311 \rangle$ axis and of length 4.75 Å. The interlayer translation vector $\vec{c}$ is directed along a close-packed $\langle 111 \rangle$ axis and the bulk interlayer spacing is 0.906 Å. The bulklike registry of one layer with respect to the next-deepest layer is given by the relation $\vec{c}_{\text{par}} = \frac{2}{5}\vec{a}_1 + \frac{3}{10}\vec{a}_2 = \frac{1}{5}a\sqrt{10}\hat{x} + \frac{1}{2}a\hat{y}$, where $\vec{c}_{\text{par}}$ is the projection of the interlayer translation vector $\vec{c}$ onto the {310} plane, and $\hat{x}$ and $\hat{y}$ are defined in Table I. The surface has one mirror plane, the {100} plane, but there are no rotational symmetries.

The low symmetry of the {310} surface (see Fig. 3) leads to the expectation that the surface relaxation will exhibit registry shifts, i.e., parallel relaxation, in addition to the usual changes in interlayer spacings, as has been found for Fe{211}.[10] For example, if atoms of the first atomic layer were to move in the direction opposite to the axis labeled $\langle 310 \rangle$ in the top view of Fig. 2 by a distance of 0.23
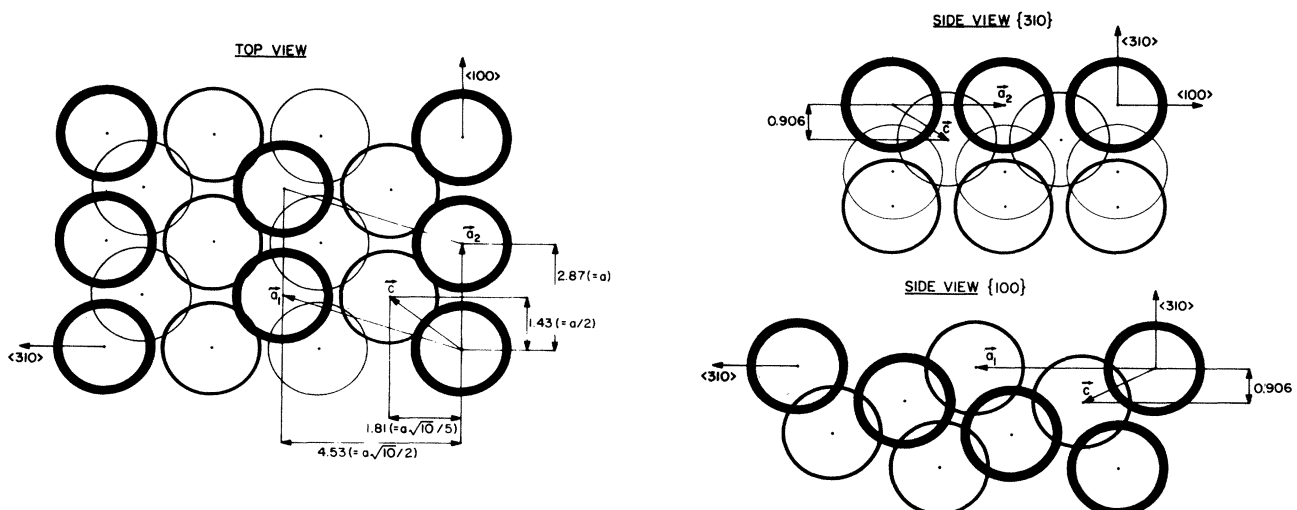

FIG. 2. Top and side views of the undistorted Fe{310} surface. Circles of equal thickness represent coplanar atoms; for the top view circles of decreasing thickness indicate progressively deeper layers. All distances are in Å.

TABLE I. Surface lattice vectors $\vec{a}_1$ and $\vec{a}_2$, parallel component $\vec{c}_{par}$ of the interlayer translation vector, interlayer distance d, and mirror plane m for the bulklike Fe{310} surface. $\hat{x}$ is along $\langle 310 \rangle$ in Fig. 2 and perpendicular to $\hat{y}$; $\hat{y}$ is along $\vec{a}_2$ and parallel to $\langle 100 \rangle$ in Fig. 2; $\hat{z}$ is directed along inward surface normal. $a = 2.866$ Å.

$\vec{a}_1$	$\frac{1}{2} a \sqrt{10} \hat{x} + \frac{1}{2} a \hat{y}$
$\vec{a}_2$	$a \hat{y}$
$\vec{c}_{par}$	$\frac{1}{5} 2\vec{a}_1 + \frac{3}{10} \vec{a}_2 \ (= \frac{1}{2} \vec{a}_2 + \frac{1}{5} a \sqrt{10} \hat{x})$
d	$a / \sqrt{10}$
m	{100}

Å, then each top-layer atom would have three nearest neighbors in the second layer as compared to two for the bulklike structure. As a result of the shift, however, the nearest-neighbor distance between atoms in the first and third layers would then be decreased and the correspond-
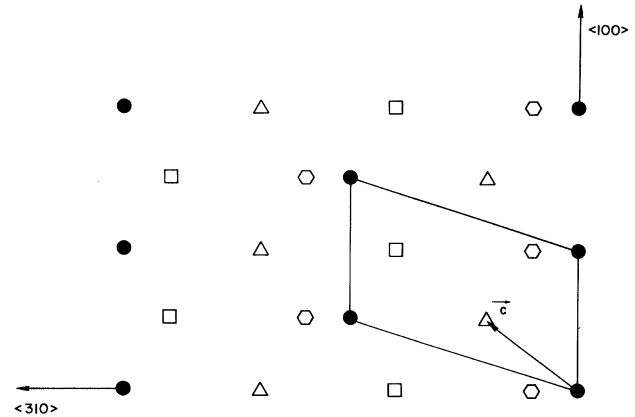

FIG. 3. Schematic representation of the first four layers of the Fe{310} surface. Solid circles: first layer. Triangles: second layer. Squares: third layer. Hexagons: fourth layer.

TABLE II. Results of calculations for $\theta = 0°$ of various structural models: d_{12}, d_{23}, and d_{34} are the first three interlayer spacings, a_{12} and a_{23} are the first two interlayer registry parameters (see text). The agreement between theory and experiment is given by the reliability factor r. All distances are in Å.

| Run	d_{12}	d_{23}	d_{34}	a_{12}	a_{23}	r
1(bulk)	0.906	0.906	0.906	1.813	1.813	0.292
2	0.880	0.906	0.906	1.813	1.813	0.280
3	0.854	0.906	0.906	1.813	1.813	0.278
4	0.854	0.933	0.906	1.813	1.813	0.219
5	0.854	0.933	0.906	2.015	1.813	0.199
6	0.854	0.933	0.906	1.611	1.813	0.250
7	0.854	0.933	0.906	2.015	1.914	0.191
8	0.854	0.933	0.880	2.015	1.914	0.171
9	0.822	0.933	0.880	2.015	1.914	0.152
10	0.822	0.933	0.922	2.015	1.914	0.162
11	0.822	0.933	0.943	2.015	1.914	0.151
12	0.801	0.933	0.943	2.015	1.914	0.137
13	0.801	0.933	0.922	2.015	1.914	0.152
14	0.801	0.933	0.880	2.015	1.914	0.144
15	0.779	0.933	0.943	2.015	1.914	0.130
16	0.811	0.943	0.943	2.015	1.914	0.144
17	0.779	0.949	0.938	2.015	1.914	0.127
18	0.779	0.965	0.938	2.015	1.914	0.129
19	0.779	0.949	0.880	2.015	1.914	0.136
20	0.779	0.949	0.880	1.964	1.914	0.125
21	0.779	0.949	0.943	1.914	1.813	0.136
22	0.779	0.949	0.901	1.914	1.813	0.124
23	0.779	0.949	0.880	1.914	1.813	0.122
24	0.779	0.949	0.880	1.939	1.813	0.120
25	0.779	0.949	0.880	1.889	1.813	0.125
26	0.779	0.949	0.880	1.864	1.813	0.130
27	0.759	1.014	0.880	1.994	1.813	0.102
28	0.759	1.014	0.880	1.964	1.813	0.100
29	0.759	1.014	0.880	1.934	1.813	0.100
30	0.759	1.014	0.880	1.903	1.813	0.102
31	0.759	1.014	0.880	1.949	1.934	0.113
32	0.759	1.014	0.880	1.949	1.874	0.100
33	0.759	1.014	0.880	1.949	1.813	0.100
34	0.759	1.014	0.880	1.949	1.752	0.113
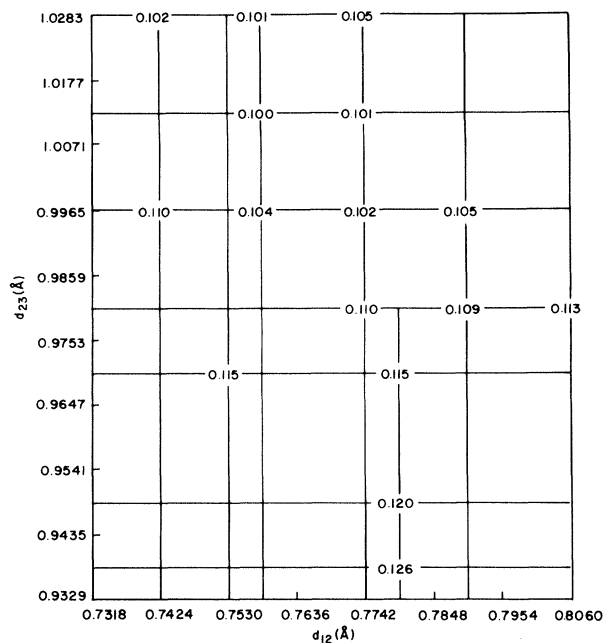
FIG. 4. Variation of the r factor for the data set at $\theta=0°$ as a function of d_{12} and d_{23} with $d_{34}=0.880$ Å, $a_{12}=1.934$ Å, and $V_0=-10.5$ eV.

FIG. 5. Schematic representation with optimized surface parameters for Fe{310}. All distances are in Å.

ing next-nearest-neighbor distances increased, which would be expected to limit the top-layer registry shift. For parallel shifts of deeper layers it is unclear even what the *signs* of the shifts might be. The purpose of the LEED intensity analysis carried out in this work was to determine the signs and magnitudes of the registry shifts and the relaxations of the interlayer spacings.

The structural parameters that were varied in the calculations were the first three interlayer spacings, d_{12}, d_{23}, and d_{34}, and the first two registry shifts a_{12} and a_{23}. (The registry shift between successive layers i and j is defined by $\vec{c}_{\mathrm{par}_{ij}}=\frac{1}{2}\vec{a}_2+a_{ij}\hat{x}$, where $\vec{c}_{\mathrm{par}_{ij}}$ is the projection of the interlayer translation vector onto the {310} plane. See Table I and Fig. 2 for definitions. The bulk value of a_{ij} is 1.813 Å.) Beginning with the bulklike structure, all d_i equal to 0.906 Å and all a_{ij} equal to 1.813 Å, a series of calculations for normal incidence were performed
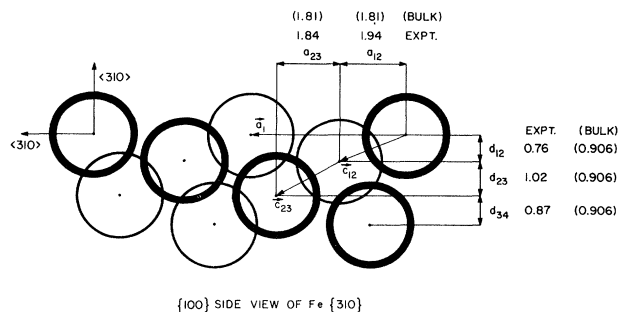
which involved independent and relatively large variations of the five structural parameters. A sampling of the calculations is shown in Table II, labeled with run numbers 1–23. The models that gave the best agreement with experiment indicated that d_{12}, d_{23}, and d_{34} were contracted ($\sim 15\%$), expanded ($\sim 5\%$), and contracted ($\sim 3\%$), respectively, compared to bulklike values, that a_{12} increased by about 5% over the bulk value and a_{23} was nearly unchanged.

Next, with d_{12}, d_{23}, and d_{34} set at 0.779, 0.949, and 0.880 Å, respectively, a_{12} was varied from 1.864 to 1.939 Å in steps of 0.025 Å (see runs 23–26 in Table II). A parabolic fit to the r factor as a function of a_{12} gave a minimum for $a_{12}=1.934$ Å. The next series of calculations varied d_{12}, d_{23}, and d_{34} independently in small steps near the above rough best values (0.779, 0.949, and 0.880 Å, respecively), with a_{12} fixed at 1.934 Å and a_{23} bulk-like. Figure 4 shows the values of the r factor for variations of d_{12} and d_{23} set to 0.880 Å (the same plot could be made for nearby values of d_{34}, but the r-factor values are slightly higher). Fitting a quadratic function of d_{12} and d_{23} (elliptic paraboloid) to the r factor gives $d_{12}=0.759$ Å and $d_{23}=1.014$ Å as optimum values. With the first three interlayer spacings fixed at the above optimum values, a_{12} was varied from 1.903 to 1.994 Å in steps of 0.030 Å (runs 27–30 in Table II), a parabolic fit to the r factor gave $a_{12}=1.949$ Å. Next, with the above best values of d_{12}, d_{23}, d_{34}, and a_{12}, calculations were made for a_{23} changing from 1.752 to 1.934 Å (runs 31–34 in

TABLE III. Results of calculations for $\theta=14°$, $\phi=-107.5°$ of various structural models: d_{12}, d_{23}, and d_{34} are the first three interlayer spacings, a_{12} and a_{23} are the first two interlayer registry parameters (see text). The agreement between theory and experiment is given by the reliability factor r. All distances are in Å.

Run	d_{12}	d_{23}	d_{34}	a_{12}	a_{23}	r
1	0.758	1.012	0.869	1.949	1.853	0.123
2	0.742	1.012	0.869	1.949	1.853	0.125
3	0.758	0.996	0.869	1.949	1.853	0.125
4	0.758	1.012	0.869	2.002	1.853	0.137
5	0.758	1.012	0.869	1.949	1.800	0.120
6	0.764	1.018	0.869	1.936	1.850	0.120
7	0.770	1.024	0.863	1.923	1.846	0.119

TABLE IV. Optimum values of structural parameters and of the real part of the inner potential V_0. ΔE equals total energy range.

Data	d_{12}	d_{23}	d_{34}	a_{12}	a_{23}	V_0	ΔE (eV)	r
$\theta = 0°$	0.759	1.014	0.880	1.949	1.841	−10.5	1704	0.098
$\theta = 14°$ $\phi = -107.5°$	0.772	1.026	0.869	1.917	1.845	−9.5	1185	0.119
Mean	0.764	1.019	0.874	1.936	1.843	−10.1	2889	

Table II). The r-factor minimum occurs for $a_{23} = 1.841$ Å. The best value of the real part of the inner potential, V_0, which was allowed to vary independently in all calculations, was determined to be -10.5 eV.

We wish to emphasize at this point that the above method for finding the overall r-factor minimum (and hence the solution to the surface structure problem) in the six-dimensional parameter space, with $r = r(d_{12}, d_{23}, d_{34}, a_{12}, a_{23}, V_0)$, is incomplete owing to the limited number of (lengthy) calculations which were feasible. The main problem is the correlation between different variables, i.e., it is not possible to vary one parameter at a time in order to optimize the structure. In analyzing the normal-incidence data for Fe{310} we have made a substantial number of calculations allowing independent variations of the three most sensitive parameters, d_{12}, d_{23}, and d_{34}, while consideration of changes in a_{12} and a_{23} were more limited. In order to take into account more accurately the correlation between registry shifts and interlayer spacings, a different strategy was used for analyzing the data at $\theta = 14°$, $\phi = -107.5°$. The method used was the following: (i) Use values of the structural parameters set near the optimum values found from analyzing $\theta = 0°$ data as initial values; (ii) vary each of the parameters one at a time by a small amount; (iii) calculate the local gradient $\vec{\nabla} r$ of the r factor as a function of the structural variables; and (iv) make a series of calculations along the direction of $-\vec{\nabla} r$ in the parameter space and find the r-factor minimum along that direction. If the surfaces of equal r factor are spherical, then $-\vec{\nabla} r$ will point exactly toward the global minimum. Problems arise when the equi-r-factor surfaces are not spherical (and they usually

are not) and/or when the r factor has multiple minima (this case is also common)—the object is to find the *deepest* minimum. The solution to the former case is obtained by recalculating the local gradient about each new minimum until the point is found where the local gradient vanishes. The latter, more difficult, case involves blanketing the parameter space with enough calculations so that the region with lowest absolute values of the r factor is found and then local-gradient method can be applied. It is clear that when there are many variables, compromises must be made which will increase the uncertainties beyond those inherent in the experimental technique.

Table III shows the calculations used to determine the local gradient of the r factor as a function of d_{12} d_{23}, a_{12}, and a_{23}. The values of d_{34} and V_0 were varied independently in each calculation since little extra computer time was required; the entries in the table are for the optimum values of 0.869 Å for d_{34} and -9.5 eV for V_0. Runs 1—5

TABLE V. r factors for the bulklike and fully relaxed models for the three experimental data sets and mean r factors for all data.

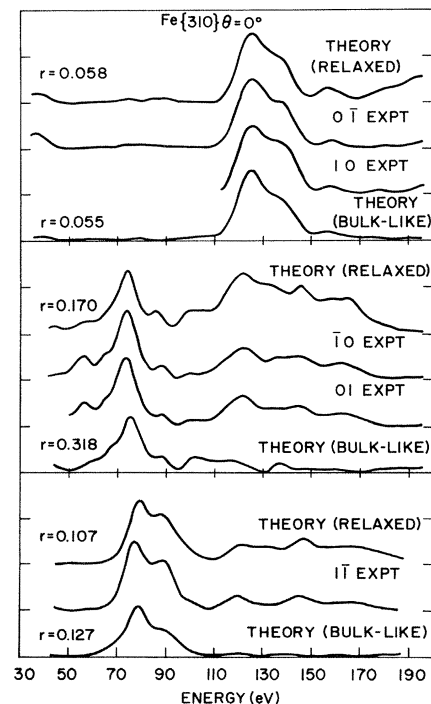| Data sets	Bulklike	Relaxed	Energy range (eV)
$\theta = 0°$	0.292	0.102	1704
$\theta = 7°$ $\phi = -107.5°$	0.193	0.126	1205
$\theta = 14°$ $\phi = -107.5°$	0.187	0.127	1185
Mean	0.232	0.116	4094

FIG. 6. Experimental and calculated LEED spectra. Theoretical curves are shown both for the bulklike and the fully relaxed model.
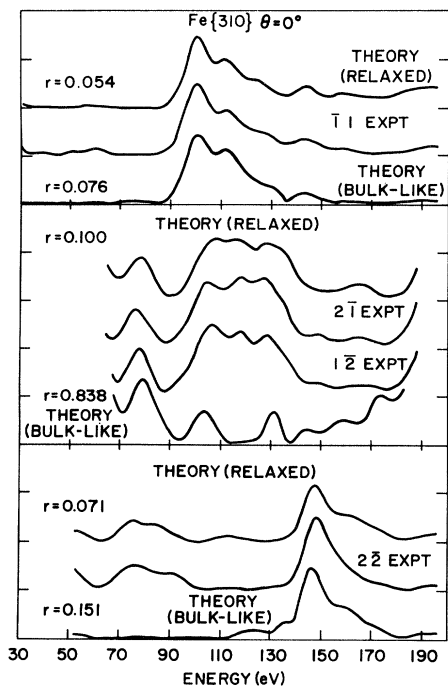
FIG. 7. Experimental and calculated LEED spectra. Theoretical curves are shown both for the bulklike and the fully relaxed model.
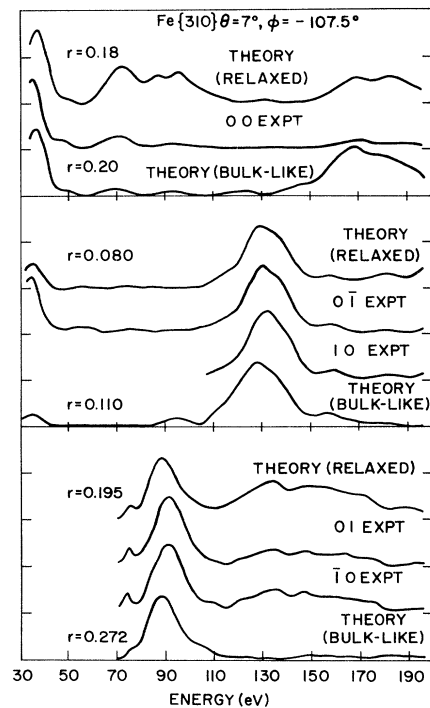

FIG. 9. Experimental and calculated LEED spectra. Theoretical curves are shown both for the bulklike and the fully relaxed model.
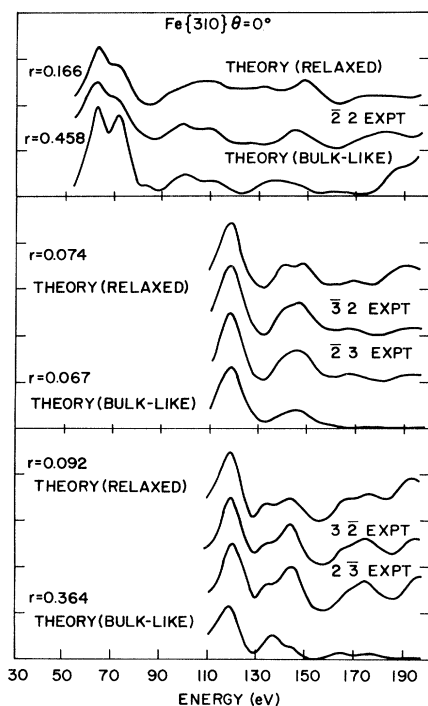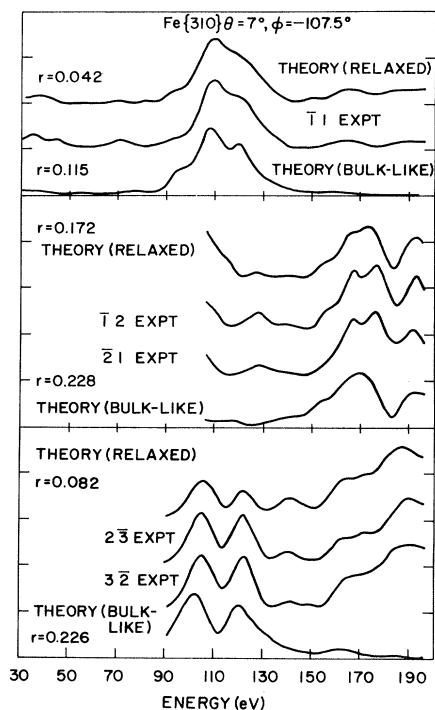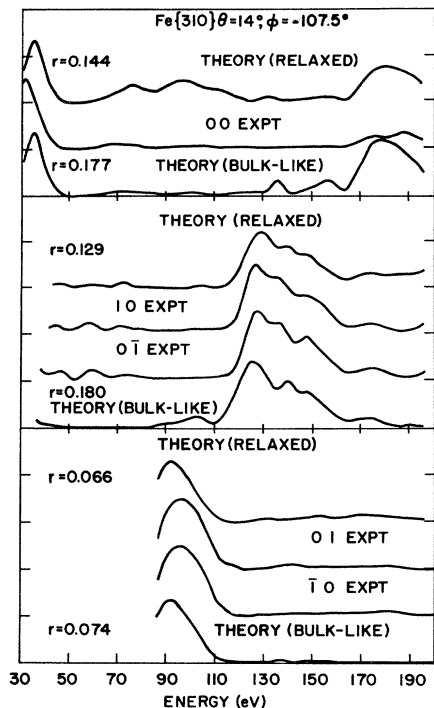

FIG. 8. Experimental and calculated LEED spectra. Theoretical curves are shown both for the bulklike and the fully relaxed model.

FIG. 10. Experimental and calculated LEED spectra. Theoretical curves are shown both for the bulklike and the fully relaxed model.

FIG. 11. Experimental and calculated LEED spectra. Theoretical curves are shown both for the bulklike and the fully relaxed model.
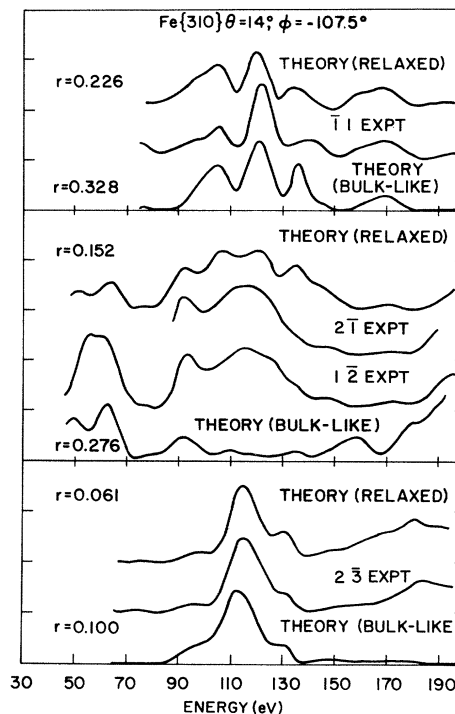

FIG. 12. Experimental and calculated LEED spectra. Theoretical curves are shown both for the bulklike and the fully relaxed model.

in Table III were used to evaluate $\vec{\nabla}r = (d_{12}, d_{23}, a_{12}, a_{23})$, and runs 6 and 7 were made along the direction $-\vec{\nabla}r$. The parameter values determined by a parabolic fit to the r factors of runs 1, 6, and 7 are given in Table IV as are the values from the $\theta=0°$ analysis and the weighted (by the total energy range of the data sets) mean values. The three decimal places recorded in the table represent the precision of the computations, not the accuracy (see below). Nevertheless, the agreement between the two data sets is very good; the values for corresponding interlayer spacings are within 0.01 Å of each other and the registry shifts are consistent within 0.03 Å. In Table V we list the r-factor values for the data at three angles of incidence for the bulklike and fully relaxed models. The spectra at $\theta=7°$, $\phi=-107.5°$ were not used in the intensity analysis owing to limitations on computer time. Figure 5 is a schematic representation of the relaxed surface structure and Figs. 6–12 show the experimental spectra together with the calculated spectra for both the relaxed and bulk-like structures. Comparison of spectra for the relaxed and bulklike models with each other and with experiment demonstrates the sensitivity of LEED; the overall improvement in agreement between theory and experiment obtained for the relaxed structure is quite striking.

In summary, the observed structure of Fe{310} is:

(i) bulk interlayer spacing 0.906 Å,
(ii) bulk layer-to-layer registry shift 1.813 Å,
(iii) $d_{12} = 0.76 \pm 0.3$ Å (16.1±3.3 % contraction),

(iv) $d_{23} = 1.02 \pm 0.03$ Å (12.6±3.3 expansion),
(v) $d_{34} = 0.87 \pm 0.04$ Å (4.0±4.4 % contraction),
(vi) $a_{12} = 1.94 \pm 0.05$ Å (7.2±2.8 % relaxation toward more symmetrical registration with respect to the second layer),
(vii) $a_{23} = 1.84 \pm 0.05$ Å (1.6±2.8 % in same direction as top-layer registry shift),
(viii) $V_0 = -10.1 \pm 1.0$ eV,
(ix) $\overline{r}_{min} = 0.116$ (Zanazzi and Jona[13] r factor, 33 spectra for a total 4094-eV energy range).

The percentage changes are with respect to the bulk values given above. The associated errors are estimates; for a discussion of errors in LEED, see Ref. 20.

The change in top-layer registry shift $\Delta a_{12} = a_{12}(\text{relaxed}) - a_{12}(\text{bulk}) = 0.13$ Å, is to be compared to the change of 0.23 Å which would place each first-layer atom in a position where it would have three nearest neighbors in the second layer as opposed to two for the bulklike registry. Thus the parallel shift of the top layer is 56% of the shift necessary to achieve maximum coordination of first-layer atoms with respect to the second layer, the shift being limited by the influence of deeper layers. The change in second registry shift is in the same direction as the first, in contrast to the case of Fe{211} (Ref. 10) where the first two changes in registry shift were found to have opposite signs. There are not enough cases known at present of parallel relaxations to determine the systematics.

---

*Also at the Department of Physics, State University of New York, Stony Brook, New York 11794.

[1]S. K. S. Ma, F. W. DeWette, and G. P. Alldredge, Surf. Sci. 78, 598 (1978).

[2]U. Landman, R. N. Hill, and M. Mostoller, Phys. Rev. B 21, 448 (1980).

[3]H. L. Davis, J. R. Noonan, and L. H. Jenkins, Surf. Sci. 83, 559 (1979).

[4]D. L. Adams, H. B. Nielsen, J. N. Andersen, I. Stengaard, R. Feidenhans'l, and J. E. Sorensen, Phys. Rev. Lett. 49, 669 (1982).

[5]H. B. Nielsen, J. N. Andersen, L. Petersen, and D. L. Adams, J. Phys. C 15, L1113 (1982).

[6]J. R. Noonan and H. L. Davis, Bull. Am. Phys. Soc. 26, 224 (1981).

[7]H. L. Davis and J. R. Noonan, Surf. Sci. 126, 245 (1983).

[8]V. Jensen, J. M. Andersen, H. B. Nielsen, and D. L. Adams, Surf. Sci. 116, 66 (1982).

[9]H. L. Davis and D. M. Zehner, J. Vac. Sci. Technol. 17, 190 (1980).

[10]J. Sokolov, H. D. Shih, U. Bardi, F. Jona, and P. M. Marcus, Solid State Commun. 48, 739 (1983).

[11]J. Sokolov, F. Jona, and P. M. Marcus, Solid State Commun. 49, 307 (1984).

[12]Packing fraction of an atomic plane is the fraction of the area of the plane occupied by atoms, where the radii of the atoms are given by the touching radius of atoms in the bulk (one-half the nearest-neighbor distance).

[13]E. Zanazzi and F. Jona, Surf. Sci. 62, 61 (1977).

[14]H. D. Shih, F. Jona, U. Bardi and P. M. Marcus, J. Phys. C 13, 3801 (1980).

[15]H. D. Shih, F. Jona, and P. M. Marcus, Surf. Sci. 104, 39 (1981).

[16]E. Zanazzi, F. Jona, D. W. Jepsen, and P. M. Marcus, Phys. Rev. B 14, 432 (1976).

[17]D. W. Jepsen, H. D. Shih, F. Jona, and P. M. Marcus, Phys. Rev. B 22, 814 (1980).

[18]D. W. Jepsen, Phys. Rev. B 22, 5701 (1980).

[19]K. O. Legg, F. Jona, D. W. Jepsen, and P. M. Marcus, J. Phys. C 10, 937 (1977).

[20]J. Sokolov, F. Jona and P. M. Marcus, J. Phys. C (in press).